A wearable diffuse reflectance sensor for continuous monitoring of cutaneous blood content

2009 Phys. Med. Biol. 54 5301

(http://iopscience.iop.org/0031-9155/54/17/015)

IOP PUBLISHING PHYSICS IN MEDICINE AND BIOLOGY

Phys. Med. Biol. **54** (2009) 5301–5320 doi:10.1088/0031-9155/54/17/015

A wearable diffuse reflectance sensor for continuous monitoring of cutaneous blood content

P Zakharov, M S Talary and A Caduff[1]

Solianis Monitoring AG, Leutschenbachstrasse 46, CH-8050 Zürich, Switzerland

E-mail: andreas.caduff@solianis.com

Received 10 March 2009, in final form 21 July 2009
Published 18 August 2009
Online at stacks.iop.org/PMB/54/5301

Abstract

An optical diffuse reflectance sensor for characterization of cutaneous blood content and optimized for continuous monitoring has been developed as part of a non-invasive multisensor system for glucose monitoring. A Monte Carlo simulation of the light propagation in the multilayered skin model has been performed in order to estimate the optimal geometrical separation of the light source and detector for skin and underlying tissue. We have observed that the pathlength within the upper vascular plexus of the skin which defines the sensor sensitivity initially grows with increasing source–detector distance (SDD) before reaching a maximum at 3.5 mm and starts to decay with further increase. At the same time, for distances above 2.4 mm, the sensor becomes sensitive to muscle blood content, which decreases the specificity to skin perfusion monitoring. Thus, the SDDs in the range from 1.5 mm to 2.4 mm satisfy the requirements of sensor sensitivity and specificity. The hardware implementation of the system has been realized and tested in laboratory experiments with a venous occlusion procedure and in an outpatient clinical study in 16 patients with type 1 diabetes mellitus. For both testing procedures, the optical sensor demonstrated high sensitivity to perfusion change provoking events. The general build-up of cutaneous blood under the sensor has been observed which can be associated with pressure-induced vasodilation as a response to the sensor application.

(Some figures in this article are in colour only in the electronic version)

1. Introduction

In vivo continuous non-invasive glucose monitoring (NIGM) has the promise of providing great relief to many patients with diabetes mellitus (DM) for whom tight glucose control is

[1] Author to whom any correspondence should be addressed.

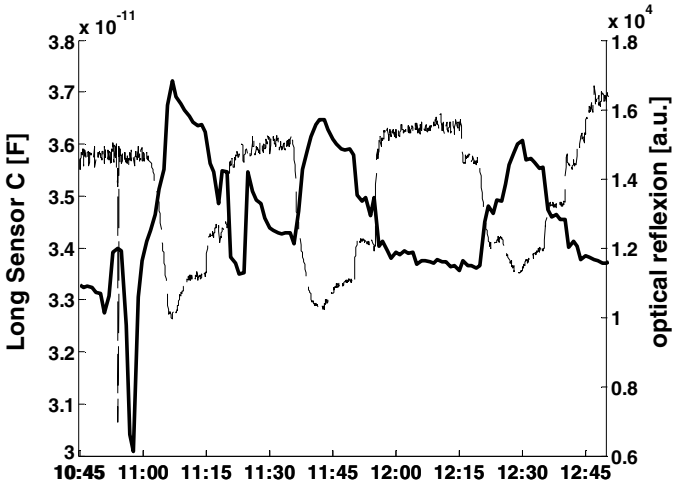

Figure 1. Comparison of skin capacitance measurements (bold line—left axes) and intensity of 550 nm light back reflected from the skin (thin line—right axes). Reproduced with permission from Talary *et al* (2007).

desirable for reducing the effects of long-term complications or helping to avoid the potentially life-threatening condition of hypoglycemia. Currently, the control of the body glucose is performed in a blood sample requiring painful puncture of the skin in order to draw a drop of blood, typically from the fingertip. For patients with DM, the American Diabetes Association recommends at least five tests per day (ADA 1999). A number of non-invasive approaches for the *in vivo* body glucose measurement based on different physical techniques have been tested and some of them have been shown to be able to follow the glucose changes under controlled laboratory/clinical conditions (Khalil 2004). Glucose variations in the human body induce a number of effects that lead to changes in the biophysical characteristics (such as optical or dielectric) of skin and underlying tissue (Talary *et al* 2007, Khalil 2004, Caduff *et al* 2004, 2009, Hayashi *et al* 2003). However, due to the complex nature of human physiology and the effect of other parameters acting as perturbations which can also affect the biophysical characteristics, a method of following these changes is required (Caduff *et al* 2009, Khalil 2004). Thus, a NIGM system suitable for the real-life conditions in home use should account for complex perturbations that affect the measurements, such as natural physiological fluctuations of the body's status (Khalil 2004). The idea underlying the multisensor glucose monitoring system (MGMS) which is under development at Solianis Monitoring AG is to monitor the most important parameters of the tissue simultaneously in order to compensate for such perturbations and to improve sensitivity and specificity of the NIGM (Caduff *et al* 2009).

1.1. Cutaneous blood content

One of the important fluctuating physiological parameters inducing significant changes in the skin status and acting as a potentially perturbing factor for NIGM is the amount of blood in the upper skin layers (Talary *et al* 2007). Figure 1 demonstrates the dependence of the glucose-related signal of skin capacitance on the cutaneous blood content (CBC) when measured with the reflection of green light.

The skin is the largest and outermost organ of the body and accounts for 10–15% of the body mass (Rhoades and Bell 2008). It has one of the lowest metabolic rates in the body and thus requires relatively low blood volume for purely nutritive functions (Rhoades and Bell 2008). However, it plays a major role in the body thermoregulation which is achieved by redirecting warm blood from the body core to the skin (Braverman 1995, Hunter *et al* 2002, Despopoulos and Silbernagl 2003), where heat transfer to the environment can occur. Thus, the amount of blood held in the skin can be tuned from almost zero to more than 5% of the total blood volume exceeding the blood flow to the muscles (Rhoades and Bell 2008). The maximum blood flow in skin can reach 5–8 L min^{-1} which is more than ten times higher than the flow at rest (Rhoades and Bell 2008, Despopoulos and Silbernagl 2003). Besides, internal or environmental temperature changes in CBC can be triggered by a number of extrinsic or intrinsic factors, such as blood pressure, blood oxygenation, heart rate, posture, exercise, external pressure, metabolic status or psychological stress (Rhoades and Bell 2008, Despopoulos and Silbernagl 2003, Scanlon and Sanders 2006). Since the skin is employed as a blood reservoir by the body, changes in the blood requirements of other organs lead to the changes in the CBC (Lima and Bakker 2005).

It should be noted that the blood content in the skin should be discriminated from the cutaneous blood flow (CBF). While under certain conditions CBF is positively correlated with CBC (Hertzman *et al* 1947), this relation does not hold in all situations. For example, when the blood flow is obstructed by venous occlusion, blood volume can increase due to arterial inflow. The measurements of NIGM are directly dependent on the tissue composition and only indirectly on the dynamics. Thus, in the further discussion, we focus on the CBC, which is a characteristic of the volume of blood in the skin layers.

1.2. Methods for CBC monitoring

It has been argued that CBC is an important physiological parameter by its own (Lima and Bakker 2005), which can serve as an indicator of body hemodynamic function. For example, in circulatory failure, blood flow is diverted from less important organs such as skin to the vital organs such as the heart, brain and kidneys. Thus, monitoring of CBC can be an early marker of the hypoperfusion of vital tissues (Lima and Bakker 2005).

A number of non-invasive techniques have been developed for the measurement of skin blood perfusion and blood content. These include measurements of the body temperature gradient between skin and environment, or skin and core body temperature or skin on the finger and on the forearm. Also the transcutaneous diffusion of oxygen and carbon dioxide can be determined through heated skin which is related to CBC. However, the major practical importance belongs to the optical methods, which probe the tissue with light in the visible and near-infrared (NIR) range, which is non-ionizing and has sufficient penetration depth. Due to the characteristic absorption spectrum of hemoglobin which is the major oxygen-transporting protein in the blood and responsible for its red appearance, its presence can relatively easily be determined and quantified in the tissue using spectroscopic techniques. As illustrated in figure 3, the spectrum of hemoglobin with an associated atom of oxygen (oxyHb) differs from the spectrum of reduced hemoglobin (rHb) significantly. Both hemoglobins along with the skin photo-protecting pigment melanin, contained in the epidermal layer, are the major absorbers of the visible and NIR light in the skin. Nevertheless, due to the high turbidity of the skin, light attenuation cannot be solely attributed to the absorption and thus quantitative interpretation of the measurement can be difficult. One of the possible solutions is provided by the dynamics of blood flow in the tissues (i.e. variations of blood content with the pulse). When relating the intensity variations induced by pulsation (AC component) to the total

detected intensity (DC component), one can estimate the contribution of the blood absorption to the total attenuation and thus determine the blood content. This is the basic principle of photoplethysmography (PPG), which is widely recognized as a robust method for pulse oximetry in the clinical environment (Allen 2007). However, this technique has a limited application for the monitoring of CBC, since only about 0.2% of the backscattered light is modulated by arterial pulsation in the reflection mode (Cui *et al* 1990) This represents a modulation level which is difficult to reliably measure on a moving subject. Moreover, the origin of the pulsating component is not limited to volume changes alone, as it has been shown to be affected by a number of other factors such as blood vessel wall movement or red blood cell (RBC) orientation (Allen 2007).

Methods based on the coherent light scattering from the tissue, such as laser Doppler flowmetry (LDF) and laser speckle imaging (LSI), also rely on the blood dynamics (Zakharov and Scheffold 2009, Lima and Bakker 2005, Nilsson *et al* 2003). Here the fluctuations of the scattered light intensity are caused by the movement of the RBCs and the speed of fluctuations is determined by the blood velocity, while the amplitude of fluctuations is related to the blood volume. LDF and LSI are widely susceptible to the distortions produced by the subject movements than PPG and thus hardly suitable for implementation in a wearable concept at current stages of these technologies.

In its turn, the method of diffuse reflectance spectroscopy (DRS) or remittance spectroscopy (Anderson *et al* 1981) relying on the absolute intensity back-reflected from the tissue can be used to quantify the relative changes of the CBC. The increase of the hemoglobin concentration in the tissue leads to the higher absorption rate and correspondingly lower diffusely reflected intensity. DRS does not rely on the short-term variations of the detected intensity, such as in PPG, LDF or LSI, it is robust (Sinichkin *et al* 2002) and can be implemented in the cost-effective way with LEDs and semiconductor photo-detectors (see e.g. Feather *et al* (1988) and Pearse *et al* (1990)). Such an implementation makes it potentially applicable in wearable devices for non-invasive CBC monitoring under the normal-life conditions.

In the current paper, we first discuss the structural peculiarities of the skin, which are important for the design of a DRS sensor. According to the skin morphology, we build a skin model for the Monte Carlo simulation of light propagation in such a scattering tissue which is used for the optimization of the sensor geometry. Based on the outcome of the simulation, we developed an optical sensor incorporated into the MGMS prototype. Performance of the system is discussed based on the results of experimental tests using the venous occlusion protocol and continuous monitoring of patients with type 1 DM (T1DM) in outpatient settings.

2. Sensor design

2.1. Skin structure and optical properties

The optical reflection sensor for blood content monitoring in the skin should be designed by accounting for the complex cutaneous morphology and the distribution of blood vasculature in the measured tissue volume.

The uppermost viable skin layer, epidermis, does not have its own vasculature and relies on the diffusive transport of nutrients from the dermal blood capillaries. As it is depicted in figure 2 in a simplified way, blood is mainly localized in two geometrically separated layers of the dermis—subpapillary or upper vascular plexus (UVP) and cutaneous or deep vascular plexus (DVP), which is located just above the subcutaneous fat. Both plexuses are interconnected by the vertical network of arterioles and venules, known as arteriovenous anastomoses (Rhoades and Bell 2008). The arterioles in the UVP form the papillary loops in

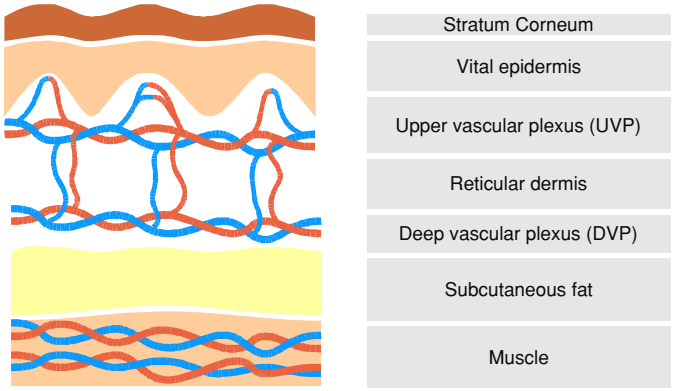

Figure 2. (a) Diagram of the skin-layered structure with distribution of blood vessels and (b) the corresponding model for simulation.

the bumpy structure of the dermal–epidermal junction, which increases the interface area with epidermis for enhanced exchange of metabolites. The UVP contains the largest part of the skin microvasculature (Braverman 1995) and is of primary importance for the thermoregulatory changes in the CBC (Hunter *et al* 2002).

The dermis is the deepest cutaneous layer followed by subcutaneous fat or subcutis which is usually the thickest layer of the skin, showing high inter- and intra-personal variations in thickness. It is mainly composed of adipocytes, a specialized cell that acts as a storage site for the fat. A limited amount of vasculature can be found in subcutaneous fat, which defines the absorption in the visible range.

On the arm, the fat layer separates the skin from the skeletal muscle tissue which is highly saturated by blood.

It is widely recognized that the performance of the optical reflection sensor for the CBC monitoring is mainly dependent on the probing wavelength range (Cui *et al* 1990) and the location of light source and detector of diffusively reflected light, determined by the source–detector distance (SDD) (Meglinskii and Matcher 2001, Meglinsky and Matcher 2001). The importance of the SDD has also been shown for the NIR-based glucose and water monitoring in the reflection mode (Arimoto *et al* 2005, Iino *et al* 2003, Yun-Han *et al* 2008).

As described above, the amount of blood can be related to the amount of hemoglobin which has a unique spectroscopic signature dependent on the state of hemoglobin oxygenation (see figure 3). The major interest for multisensor monitoring is the total amount of blood with both oxygenated and reduced hemoglobins, thus measurements have to be performed in the spectral bands were oxyHb and rHb have equal absorption efficiency, which are called isosbestic points (Gordy and Drabkin 1957). In the visible and short NIR range, such points exist around 506, 543, 550, 568, 585 and 798 nm (Prahl 1999), which can be potentially used for blood content characterization. Cui *et al* have demonstrated that green light has the maximum sensitivity and a higher signal-to-noise ratio when CBC is measured (Cui *et al* 1990). Moreover, high absorption rate of the green light by the blood can limit the penetration depth (Sandberg *et al* 2005), reduce the dependence on the muscle blood perfusion and thus increase specificity of the optical sensor to the CBC.

The other important skin absorber, melanin, has a spectrum with no particular features in the visible and NIR range. The power-law decay with a scaling exponent of -3.33 is

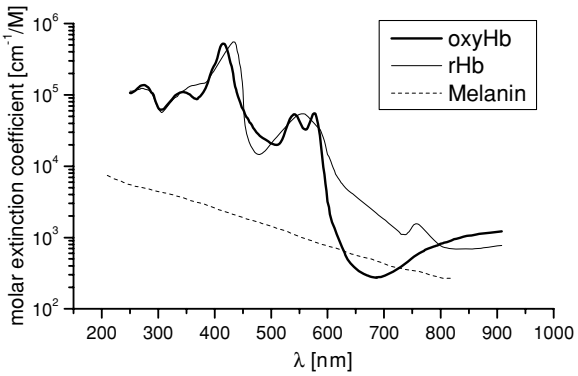

Figure 3. Molecular extinction coefficients of major skin absorbers in the visible and NIR range: melanin, oxygenated (oxyHb) and reduced (rHb) hemoglobins.

usually assumed as a good approximation of the absorption spectrum (Meglinski and Matcher 2002). Thus, melanin attenuates shorter wavelengths with higher efficiency than the longer ones.

Absorption is not the only process affecting light attenuation in biological tissue in general and skin in particular. Different natural variations such as changes in the tissue-scattering properties, morphology and Fresnel reflection from the skin surface related to the changes of the moisture content can induce significant perturbations in the detected intensity back-reflected from the skin. With a portable spectroscopic system using light sources of fixed wavelengths (like LED), these optical perturbations can be accounted by choosing the second probing wavelength with lower sensitivity to the signal of interest but with the similar response to the perturbation(s). Light of an isosbestic wavelength of 798 nm is significantly less absorbed by both hemoglobins and can serve as a reference wavelength to improve system specificity to CBC changes by compensating for the optical perturbations.

For the reasons presented above, in further analysis we concentrate on 568 nm as a signal wavelength for CBC monitoring and 798 nm as a reference wavelength and investigate the optimal SDD for the improved sensitivity and specificity to the CBC.

2.2. Theoretical considerations

As it has been mentioned previously, blood in the skin is restricted to certain compartments of the viable dermis (see figure 2). Thus, the geometry of the sensor (i.e. distance from source to detector) can be chosen according *a priori* knowledge of the skin morphology in order to increase the sensitivity to the tissue volume of interest and decrease effects of other compartments. This can be efficiently performed with a Monte Carlo simulation of the photon propagation in a model of stratified medium representing the skin and the underlying tissues (Meglinski and Matcher 2002, Meglinskii and Matcher 2001, Meglinsky and Matcher 2001).

In a reflectance experiment, light of known intensity I_0 enters the medium at the source location and the intensity I of light diffusely reflected from the sample surface is measured at the detector point. The wavelength-dependent light attenuation $A(\lambda) = -\ln[I(\lambda)/I_0(\lambda)]$ is used to characterize concentration changes of substances related to absorption of the sample. The Beer–Lambert law which relates light attenuation to the absorber concentration for the

case of reflection measurements has to be rewritten into a modified form (Delpy *et al* 1988, Hiraoka *et al* 1993b):

$$A(\lambda) = D(\lambda)\mu_a(\lambda) + G, \tag{1}$$

where $D(\lambda)$ is a wavelength-dependent effective path length, $\mu_a(\lambda)$ is the absorption coefficient and G is a loss factor, independent of absorption and related to static scattering and measurement geometry. Differentiation of equation (1) with respect to $\mu_a(\lambda)$ gives $D(\lambda) = \partial A(\lambda)/\partial\mu_a(\lambda)$, which defines the experimental way to estimate $D(\lambda)$ which is also called differential pathlength (DP) (Delpy *et al* 1988).

Typically, biological tissue has a complex structure, consisting of physiological compartments with specific optical properties and well-defined amounts of substances under investigation. The layered structure of human skin is a typical example of such a medium with blood localized in the specific layers.

In such a way, the absorption changes are limited to the certain volume V and a partial differential pathlength $D_V(\lambda)$ (PDP) within the volume should be used to characterize sensitivity (Hiraoka *et al* 1993a). The PDP corresponds to a statistical average of the paths of detected photons inside the volume of interest V:

$$\partial A(\lambda)/\partial\mu_a(\lambda) = D_V(\lambda). \tag{2}$$

The problem of the sensitivity optimization is to maximize the measured response in attenuation $A(\lambda)$ to the nominal change in the substance volume fraction Δc_i and, correspondingly, absorption coefficient $\Delta\mu_a(\lambda) = \mu_i(\lambda)\Delta c_i$. According to equation (2), sensitivity is defined by the $D_V(\lambda)$ and thus by investigating the PDP dependence on the SDD, we can find the distance maximizing the PDP in the volume of interest and minimizing PDP in other volumes. This can be efficiently performed with Monte Carlo simulations.

It should be noted that the pathlengths are assumed to be independent of the absorption in our model. However, with a significant alteration in the optical properties, the pathlengths can be modified. This will introduce a nonlinear dependence of the attenuation on the absorber concentration. Since the task of sensor optimization implies maximization of sensitivity to the small variations of CBC, we can assume the pathlength to be constant.

2.3. Monte Carlo model

The optical layered model of the skin has been derived from a review of several relevant publications (Meglinski and Matcher 2002, Meglinskii and Matcher 2001, Meglinsky and Matcher 2001). In our seven-layer model, we separate the skin and underlying tissue into the following layers: stratum corneum, vital epidermis, UVP with capillary loops, reticular dermis, DVP, subcutaneous fat (subcutis) and muscles. All of the layers were assigned with individual optical and geometrical parameters (see table 1 for detailed information), which were found in the literature (Meglinski and Matcher 2002, Meglinskii and Matcher 2001, Meglinsky and Matcher 2001, Bashkatov *et al* 2005, Cheong *et al* 1990, Douven and Lucassen 2000, Svaasand *et al* 1995, Gambichler *et al* 2006) with particular focus on the skin of the arm. Since the thickness of the fat layer is a subject of high inter-personal variability, we adopted two values for this parameter: 1 mm (thin subcutis model) and 6 mm (thick subcutis model). Thickness of the muscle layer was set to infinity as the deepest layer of the model.

Absorption of the skin layers is assumed to be defined by the absorption spectra of blood, melanin and wavelength-independent background absorption of other tissues, which is fixed to $\mu_a^0 = 0.025\ \text{mm}^{-1}$ (Svaasand *et al* 1995). Absorption of triglycerides and water was not included explicitly since it is relatively low in the analysed wavelength region.

Table 1. Morphological and optical properties of the skin layers in the simulation model.

				μ_s (mm^{-1})				
K	Name of layer	d (mm)	C_b	568 nm	798 nm	μ_a (mm^{-1})	g	n
1	Stratum corneum	0.02	0.00	0.025	0.025	100	0.86	1.50
2	Living epidermis	0.08	0.00	1.114	0.283	45	0.80	1.34
3	Upper vascular plexus with papillary loops	0.10	0.20	0.567	0.035	35	0.95	1.39
4	Reticular dermis	1.50	0.04	0.133	0.027	25	0.80	1.40
5	Deep vascular plexus	0.20	0.10	0.296	0.030	30	0.95	1.38
6	Subcutaneous fat	1.00/6.00	0.05	0.161	0.027	5	0.75	1.44
7	Muscle	∞	0.40	1.109	0.044	53	0.95	1.37

Absorption of stratum corneum as blood and melanin-free tissue is solely defined by background absorption: $\mu_a^{SC} = \mu_a^0$.

Absorption of the melanin-containing epidermal layer can be estimated using the following empirical relation (Svaasand *et al* 1995, Douven and Lucassen 2000):

$$\mu_a^{\mathrm{LE}}(\lambda) = \mu_a^{\mathrm{LE}}(694)\left[\frac{694}{\lambda}\right]^4 + \mu_a^0,$$

where λ is defined in nanometers and $\mu_a^{LE}(694)$ is the absorption coefficient for the living epidermis at 694 nm which depends on the skin type and usually in the range 0.3–2.5 mm^{-1} (Svaasand *et al* 1995). For our model, we have chosen a value of 0.5 mm^{-1} which is above the minimal value for the fair Caucasian skin.

For the blood-containing layers, absorption depends on the blood concentration C_b in the particular layer:

$$\mu_a^B = C_b F_{\mathrm{Hb}} F_{\mathrm{RBC}} \mathrm{Ht} \mu_a^{\mathrm{Hb}}(\lambda) + (1 - C_b)\mu_a^0,$$

where $F_{\mathrm{Hb}} = 0.25$ is the volume fraction of hemoglobin in RBCs, $F_{\mathrm{RBC}} = 0.99$ is the volume fraction of RBCs in the total volume of all blood cells and $\mathrm{Ht} = 0.45$ is hematocrit (Meglinski and Matcher 2002). The blood parameters are assumed to be layer independent and the concentrations are listed in table 1.

The scattering parameters μ_s and g were assumed to be constant for the analyzed spectral range in line with the model of Meglinski *et al* (Meglinski and Matcher 2002) who investigated different aspects of Monte Carlo simulations of the skin and found that the spectrum of the skin reflectance in the visible and short-wavelength NIR regions can be accurately simulated using wavelength-independent scattering properties. The calculated optical properties used for the simulation are shown in table 1.

The multilayer code is based on the published algorithm by Wang *et al* (1995), where the technical details of the Monte Carlo simulation procedure can be found. In brief, the method utilizes the photon packet approach, where the weight of the single packet is adjusted due to absorption of the medium. The Henyey–Greenstein phase function is used to simulate the scattering angle. The point illumination model is used. The original model is extended with the angle selection of the incident and reflected light, reproducing the limited numerical aperture (NA) of the source and detector. For each photon propagating in the medium, the depth history of pathlength is recorded. A photon is considered as detected when it leaves the medium by crossing the upper surface and the exit angle is within the detection limits defined by the NA. The averaged depth history for SDD equal to the photon exit distance from the source is adjusted with the weight of the packet. In this way, the pathlength statistics is

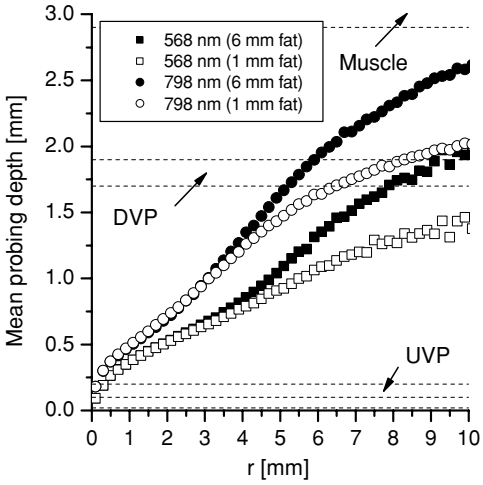

Figure 4. Averaged measurement depth as a function of source–detector distance r for 568 nm (squares) and 798 nm (circles). Filled symbols—normal thickness of fat layer (6 mm); open symbols—reduced thickness (1 mm). Dashed lines show the boundary of the layers and labels indicate the vascular plexuses of the skin.

accumulated directly and simultaneously for all SDDs and depths in a single run. Multiple runs with tuning of absorption coefficients are not required which represents an advantage over differential techniques of pathlength estimation (Hiraoka *et al* 1993b, Yun-Han *et al* 2008).

The intensity of the detected light as a function of SDD is also recorded for the analysis of signal attenuation.

For each simulation run, we have used 10^7 photon packets. The effect of numerical aperture has been analyzed by comparing results with normal incidence and unrestricted angle detection with results from the model reproducing system with LED illumination and a PiN-diode as the detector (illumination NA of 0.6 and detection NA of 0.87).

2.4. Mean probing depth

As it is common to analyze the sensitivity of the optical sensor in terms of the penetration depth, we first present the results of the simulation as the average depth visited by the detected photons also called a probing depth and we explore its dependence on the SDD. Figure 4 shows the averaged probing depth for the two analyzed wavelengths. For $r < 4$ mm, no dependence on the subcutis thickness can be seen in both wavelengths, while for higher SDD, it starts to influence the data significantly. As clearly observed, the depth is steadily increasing with distance. When relying on this quantity one can conclude that the averaged detected photon reaches the upper plexus already at minimal SDD. For the 6 mm subcutis model, the DVP can be reached with the average infrared photon for SDD above 5.0 mm and with average green photon above 8 mm. For the model with 1 mm subcutis, the SDD limit for infrared is slightly shifted to 6.5 mm, while for green light the mean probing depth does not reach the DVP within the analyzed range up to 10 mm. For the same range, the mean probing depth is within the skin and subcutis limits for both wavelengths and both thicknesses of the fat layer. This could lead to the conclusion that the changes of blood content in the muscle cannot be detected

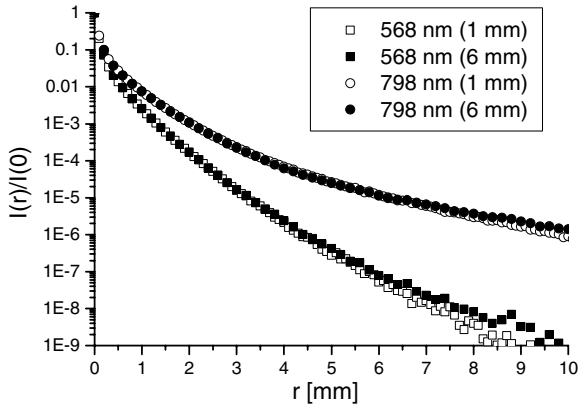

Figure 5. Simulated dependence of the intensity back-reflected from the skin model on the sensor–detector distance for two wavelengths.

by an optical system with $r < 10$ mm. Thus, the analysis of the measurement depth alone suggests that the optimal SDD for the maximal sensitivity to UVP is below 0.5 mm, while the measurements of the DVP are possible, starting from 5.0 mm, and significantly dependent on the amount of subcutaneous fat.

2.5. Spatial intensity distribution

Figure 5 presents the distribution of back-reflected light intensity for two wavelengths normalized to the intensity at $r = 0$. As one can see, the intensity decays rapidly with distance especially for the green wavelength. At around $r = 3$ mm, we observe a level of 2×10^{-5} of the initial intensity, while it remains ten times higher for the infrared intensity. This is due to the higher absorption rate of the green light. Since the LEDs operating in the green spectral range typically have a limited power, we should minimize the SDD in order to increase the signal-to-noise level of the primary.

2.6. Total differential pathlength

The sensitivity of the optical system can also be analyzed in terms of the total DP. The corresponding plots obtained for our model are presented in figure 6, where one can observe an almost linear increase of the DP with SDD. However, the slope of the trend depends on the wavelength—with the highest increase rate for the infrared light. From this result, we can conclude that the sensitivity to the absorption changes in the bulk tissue volume is linearly increasing with distance which is in agreement with results of the analytical prediction of photon diffusion theory (Pearse *et al* 1990), similar Monte Carlo simulations (Meglinsky and Matcher 2001, Iino *et al* 2003) and experiments (Kumar and Schmitt 1997). For both wavelengths within the range of analyzed SDDs, we do not observe significant differences between models with thick and thin subcutis.

2.7. Partial differential pathlengths

As discussed above, the optical system for CBC monitoring should be specifically sensitive to the blood-containing layers, thus we analyze the optical paths within these layers. The

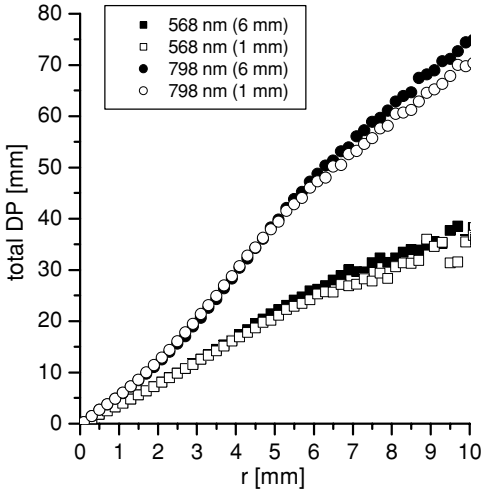

Figure 6. Total differential pathlength (DP) inside the skin as a function of source–detector distance according to simulation results.

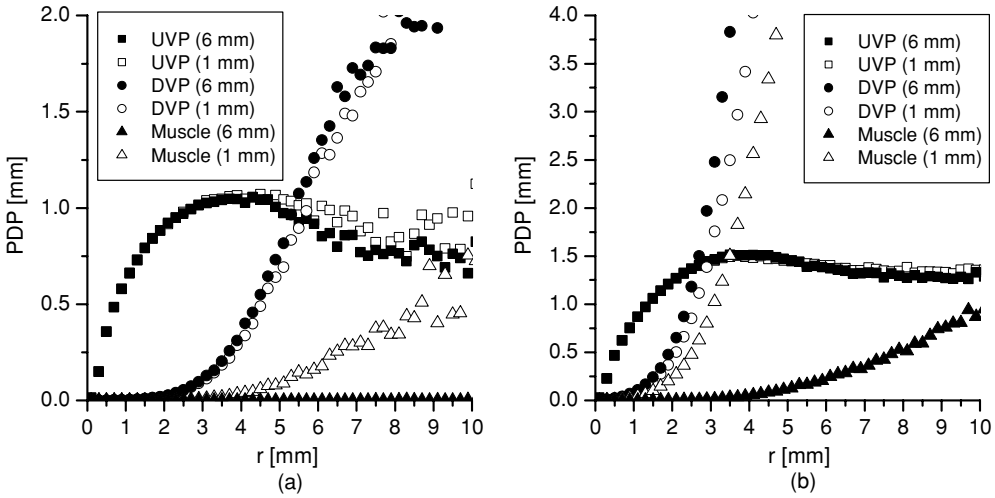

Figure 7. Partial differential pathlengths (PDP) for the light of 568 nm wavelength (a) and 798 nm (b) within the blood-containing layers of the model: upper vascular plexus (UVP—boxes), deep vascular plexus (DVP—circles) and muscle (triangulars). Filled symbols indicate the normal fat thickness (6 mm) and open symbols indicate reduced thickness (1 mm).

corresponding results are presented in figure 7(a) for the green light and in figure 7(b) for infrared. For SDD below 3 mm, the data are in agreement with observations presented above—sensitivity, characterized by the PDP increases with the r. However, within this range, the rate of growth is not constant: for the distances below 1 mm, sensitivity grows steadily with r for UVP layers and for both wavelengths, where the rate of growth starts to drop. Further increases of PDP continue until a SDD value of around 3.5 mm, where the maximum is reached and PDP starts to decline with SDD. The point of maximum corresponds to the situation when the light emitted by the source on its way to the detector propagates mostly

through the UVP layer. Further increases of r cause the propagation depth to increase; thus, photons have to cross the corresponding layer and propagate through the deeper layers and cross the UVP on their way back to the detector. Obviously, the effective pathlength in UVP is shorter in this regime. PDP dependence in the UVP layer is similar for both wavelengths: it reaches the half of the maximum value at $r \approx 0.8$ mm and 75% of the maximum at $r \approx 1.5$ mm and does not depend on the fat layer thickness.

In contrast, light propagation in the DVP layer demonstrates significant dependence on the wavelength. The pathlength for green light is almost zero for $r < 3.0$ mm, and grows rapidly after this distance, while for infrared the same can be observed starting from $r = 1.5$ mm. Such a difference in the sensitivity to the blood amount in the DVP can be a problem for the interpretation of measurements obtained with both wavelengths. In addition, for the infrared light, changes of the fat layer induce significant variations of the pathlength in DVP.

The pathlength in the muscle layer demonstrates even higher dependence on the subcutis thickness. For the green light, it remains almost zero for the whole PDP range for the thick subcutis model and remains low for the thin subcutis for SDD below 4 mm. For the infrared light, a similar behaviour can be observed in the normal-fat regime. However, for the thin subcutis muscle, PDP starts to increase from the shortest SDD and even exceeds the pathlength in UVP for $r > 3.5$ mm. This indicates the light propagation regime, when the deeper part of the banana-shaped sensitivity volume touches the muscle layer.

Since the muscle perfusion is not directly related to the CBC, sensitivity of the optical sensor to the blood content changes in the muscle can significantly disturb measurements of the CBC. Thus, a source–detector placement that allows for the high pathlengths in the muscle even for the skin with a low fat content should be avoided. This determines the upper SDD boundary of $r = 2.4$ mm when the PDP within the muscle layer reaches 25% of the maximal PDP within UVP.

It should be noted that the average measurement depth discussed above (figure 4) is below the thickness of skin together with subcutaneous fat (2.9 mm) even for the low-fat type. This result might lead to the aberrant conclusion that the muscle layer is unreachable with the suggested system geometry. However, this is in contradiction with the conclusions based on the PDP estimation. Thus, the average measurement depth is not a sufficient quantity for the description of probing depth in the layered scattering medium like the skin.

In summary, the simulation results suggest that the PDP in the UVP for both wavelengths increases rapidly with SDD up to around 3.5 mm, where it reaches its maximum and starts to decrease. The effect of light propagation within DVP is negligible for $r < 3.0$ mm, but PDP starts to rapidly increase from SDD around 4 mm. At the same time for the model with a thin layer of subcutaneous fat, infrared light propagation in the muscle increases even faster and cannot be ignored for the SDD from 2.4 mm where it reaches around 25% of the pathlength in UVP, which results in a specificity to CBC of approximately 75%.

Thus, the lower SDD limit of 1.5 mm is set by the requirements to sensitivity of the green light reflection to the blood content changes in the skin, while the upper limit of 2.4 mm is set by the requirements of the specificity of the infrared reflection to the CBC. These findings define the range of 1.5–2.4 mm as the optimal range of SDD for the monitoring of the blood content in the skin using the proposed optical settings.

2.8. Effect of the source and detector numerical aperture

In order to assess the effect of angle selection of the incident and reflected light on the light propagation, we performed the simulations in a skin model with cone illumination ($NA = 0.60$) and limited detection aperture ($NA = 0.87$). Results are presented in figure 8 together

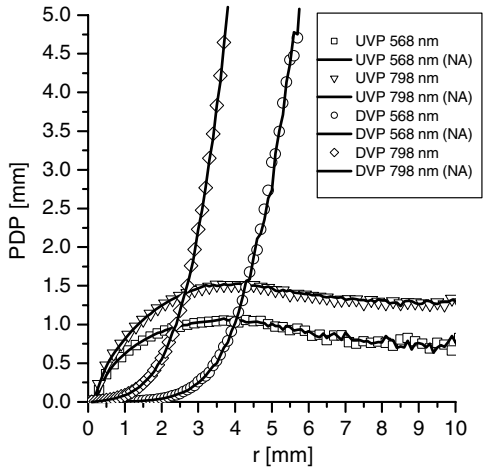

Figure 8. The simulated partial differential pathelengths within upper vascular plexus (UVP) and deep vascular plexus (DVP): comparison of the regime with normal illumination and full-angle detection (symbols) with cone illumination and limited aperture detection (lines). Skin model with subcutis thickness of 6 mm has been used.

with the results with no angular selection. It can be clearly seen that no differences in the light propagation in the blood-containing layers in the skin can be observed under the explored conditions. The reason for this might be scattering in the stratum corneum and epidermis, which randomizes the input and output angle and thus angle selection does not affect the results.

3. Experiments

3.1. Hardware implementation and data processing

Based on the results of these simulations, the optical module designed by CiS Forschungsinstitut für Mikrosensorik und Photovoltaik GmbH (Germany) is employed in the MGMS. The module depicted in figure 9 contains two LEDs with peak wavelengths $\lambda_S = 568$ (signal) and $\lambda_B = 800$ nm (baseline). The detection of light diffusely reflected by the skin is performed with a semiconductor PiN-diode and measured with the analog-to-digital converter. The distance from the LEDs to the adjacent border of the PiN-diode is 1.5 mm and to the distant border is 3.7 mm. Since the back-reflected intensity decreases rapidly along the PiN detection range, we can determine the effective SDD, as the mean distance from LEDs of the photons arrival to the PiN-diode according to the simulations (see figure 5). For the green light, we obtain 1.90 mm, and for infrared, 2.04 mm. The effective SDD is larger for infrared since it is absorbed less in the skin and its intensity decays less with distance.

Three independent optical modules are embedded into the sensor base of the functional model of the MGMS. The MGMS is equipped with controller electronics and battery, which allows it to acquire data and transfer it via the wireless link to the personal digital assistant (PDA) for temporal storage and further transfer to the personal computer (PC). The MGMS can also be directly connected to PC via universal serial bus (USB) and data can be transferred in real time with a specially designed PC software. The measurements are performed with a 20 s periodicity. Each measurement cycle is organized in the following order:

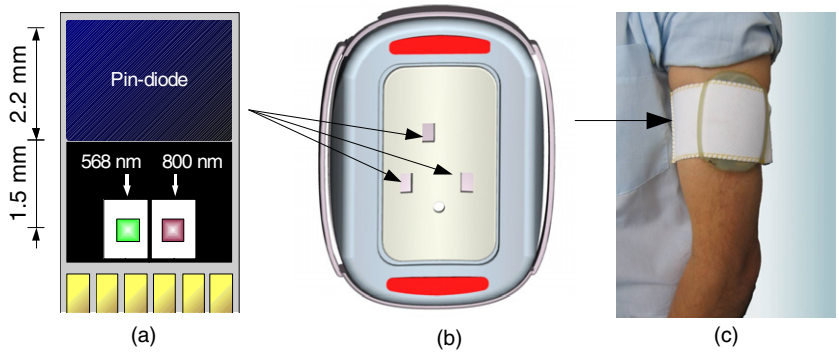

Figure 9. Hardware implementation of the optical module for non-invasive cutaneous perfusion monitoring. (a) Optical sensor; (b) placement of the optical sensors on the MGMS sensor plate; (c) MGMS attached to the arm of the patient in the outpatient study.

(1) PiN-diode measurements with only green LED turned ON (green channel): $I_M(\lambda_S)$
(2) PiN-diode measurements with all LEDs turned OFF (dark channel) I_{DK}
(3) PiN-diode measurements with only infrared LED turned ON (infrared channel): $I_M(\lambda_B)$

All three optical sensors measure simultaneously. Since the distance between sensors exceeds 15 mm, the inter-sensor cross-talk is negligible due to the high light attenuation in the skin (compare the back-reflected intensity in figure 5 at 1.5–2.4 mm range and at 10 mm). The intensity emitted by LEDs is temperature dependent; thus, the temperature T is monitored with the embedded temperature sensor located in the vicinity to the optical modules. The temperature coefficients α are estimated for each optical module independently in the temperature tests made in an oven. Using the estimated temperature dependence, the measured intensity I_M is adjusted to the standard temperature $T_s = 35\,^{\circ}\mathrm{C}$. Also the wavelength-dependent intensity of stray light $I_{SL}(\lambda)$ propagating from the LED to the PiN-diode through the sensor structure is characterized individually for each module and subtracted from the measured intensity along with the ambient light I_{DK} that is measured on-line. Corrected intensities were normalized with the reflectance I_0 of the scattering standard (polyoxymethylene block):

$$I_N(\lambda) = \{I_M(\lambda)[1 - \alpha(T - T_s)] - I_{SL}(\lambda) - I_{DK}\}/I_0(\lambda).$$

The normalized intensities $I_N(\lambda_S)$ and $I_N(\lambda_B)$ are used to calculate the blood content index (BCI) for each of three sensors independently using the following formula:

$$\mathrm{BCI} = -10\ \log_{10}\left[\frac{I_N(\lambda_S)}{I_N(\lambda_B)}\right]. \tag{3}$$

If the BCI is rewritten in the natural logarithms, it can be simplified in terms of attenuations:

$$\mathrm{PI} = -4.34[\ln I_N(\lambda_S) - \ln I_N(\lambda_B)] = 4.34[A(\lambda_S) - A(\lambda_B)]. \tag{4}$$

According to equations (1) and (4), subtraction of the baseline attenuation $A(\lambda_B)$ from the signal attenuation $A(\lambda_S)$ in calculation of BCI allows us to correct for the absorption-independent attenuation component G, related to scattering and geometrical factors. This is similar to the two-wavelength approach proposed by Diffey *et al* for the erythema calculation (Diffey *et al* 1984, Sinichkin *et al* 2002).

Indices are calculated for each sensor independently and the averaged value is used in order to reduce the effects of skin heterogeneous structure.

3.2. Experimental procedure

Experimental testing consisted of internal laboratory tests on the investigator and in an experimental/clinical study within an outpatient setting performed by Solianis Monitoring AG in patients with T1DM.

3.2.1. Venous occlusion experiments. Internal laboratory tests were performed using the procedure of venous occlusion, as described e.g. by Hamaoka (Hamaoka *et al* 2007) in order to characterize the device response to the induced changes of the CBC and were evaluated with a standardized protocol. The device was attached to the volar side of the left lower arm of three healthy volunteers. Slight variations of the device initial placement (within the area of 50 mm diameter) from one experiment to another were allowed. The pressure cuff was placed on the upper arm and has been used to restrict the venous blood flow from the arm. Pressure levels below systolic pressure of the subject have been used (i.e. 20, 40 and 60 mmHg). Such pressure levels are insufficient to block inflow while the outflow is impeded by the pressure cuff. Thus, the venous occlusion is induced, which results in continuous build-up of the blood volume in the arm due to incoming arterial blood. We have applied the occlusion for 3 min with probed pressure, followed by 2 min of zero pressure, until continuing with the application of the next pressure level. The MGMS was attached to the arm 30 min prior to the experiment and the measurements started 2 min before the start of the first occlusion. In total, the procedure took 25–30 min. During the whole experiment, the lower arm has been kept on the desk at rest, while the subject remained in a sitting position. Data were transferred via a USB cable to a PC for real-time display and further data processing.

3.2.2. Outpatient study. An outpatient study has been carried out by Solianis Monitoring AG with nine male and seven female patients with T1DM (age mean $\pm$ SD; 38.7 $\pm$ 11.8 years; body mass index: 23.8 $\pm$ 2.7 kg m^{-2}; duration of diabetes 20.1 $\pm$ 13.3 years; HbA1c: 6.8 $\pm$ 0.8%). All the patients were of Caucasian origin and skin type and showed no signs of the dermatological problems or diabetes-related complications in the area of device placement. Patients have been supplied with the MGMS and the PDA for data collection. The patients attached the device on the dorsal side of the upper arm in the morning and took it off in the evening before going to bed. The MGMS was continuously measured during the day, when patients were following their normal life activities at home, at work and outside. The device was configured to recognize the contact to the skin and measure while attached to the arm. The patients were instructed to take notes of their activities. Acquired data were uploaded to an FTP server after each study day. Each patient performed at least 10 days of measurements spanning from August till November 2008.

3.3. Experimental results and discussion

3.3.1. Venous occlusion experiments. Figure 10(a) presents typical values of the BCI during the venous occlusion test performed in the laboratory. The baseline pulsation-related variations of the measured BCI estimated before start of the pressure-cuff experiment were in the order of 0.03 $\pm$ 0.01 dB (the indicated error here and further corresponds to the 95% confidence interval).

The blood content increase induced by the venous occlusion is well resolved for the cuff pressures above 40 mmHg. Higher pressure corresponds to the higher response in the optical signal, which can be seen in figure 10(b). Sensors have demonstrated reproducible signal response of 1.38 $\pm$ 0.13 dB for 60 mmHg for all tested subjects. Inter-subject variability

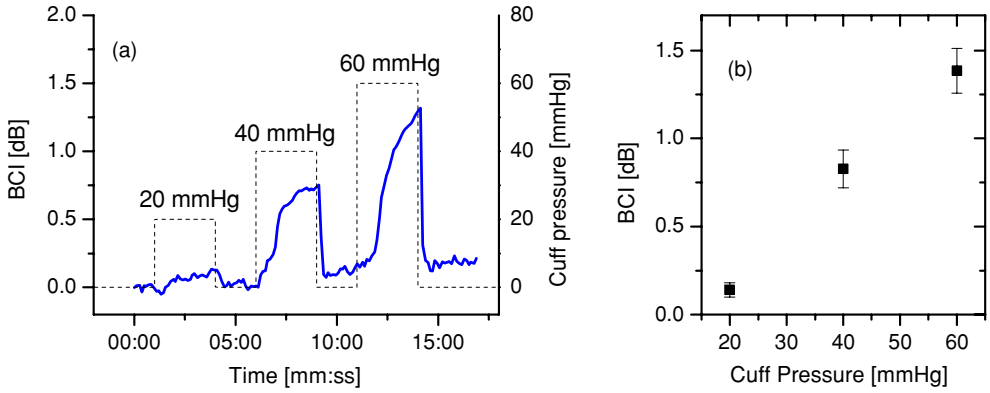

Figure 10. (a) Change of the cutaneous blood content index (BCI) during the venous occlusion experiment (solid line). Dashed line indicates the cuff pressure. Data illustrate a single experiment. (b) BCI change as a function of applied pressure averaged all other experiments. Error bars indicate standard error.

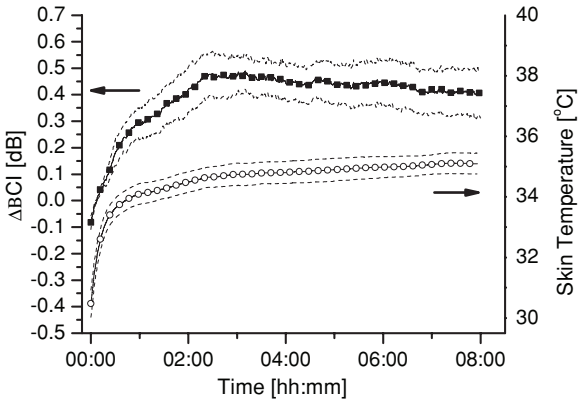

Figure 11. Change of the blood content index (BCI, filled squares) and skin temperature (open circles) during first 8 h after sensor application averaged all other subjects in outpatient study. BCI was adjusted to personal baseline for each patient estimated other first 10 min after sensor application. Dashed lines indicate limits of standard error 95% confidence interval.

expressed as a standard error of the response of 0.13 dB is only slightly larger than the sensitivity variation for a single subject (0.10 dB), which indicates that the device performance is comparable for different subjects. The intra-subject variability which is higher than the baseline noise might be related to the differences in the pressure-cuff and sensor placements.

3.3.2. Outpatient study. Figure 11 shows the BCI changes on the upper arm of subjects performing normal daily activities as a function of time elapsed from the MGMS attachment. Data from all 16 participants of the study are averaged after adjusting to the personal baselines estimated during the first 10 min.

As one can observe, the BCI increases initially after MGMS placement on the arm. The maximum BCI level of 0.490 $\pm$ 0.129 dB is reached after around 3 h after the start. The minimal single patient averaged BCI change in 3 h was 0.293 $\pm$ 0.060 dB and the

maximal 0.753 ± 0.107 dB. The results suggest that the observed effect is reproducible and quantitatively depends on the patient.

The maximum of BCI is followed by a slow decay till the end of the observation. However, the BCI does not reach the minimum level again, recorded immediately after device attachment to the arm.

The mechanism which might induce a continued increase in the CBC is the local heating of the skin under the sensor (Barcroft and Edholm 1943, Charkoudian *et al* 2002, Minson *et al* 2001). Figure 11 also shows the average change in the skin temperature under the sensor during the initial 8 h of the study day. It illustrates that the temperature increases rapidly up to 34 °C during the first 30 min, which is caused by the device warming up and then slowly progresses toward the level of 35 °C during following hours. This trend itself can be caused by the accumulation of blood under the sensor or circadian rhythms of the core body temperature. In most cases, skin temperature reached its maximum at around 16:00–20:00 after which it started to decline, which is in agreement with the known trends of body temperature (Rhoades and Bell 2008). The skin temperature level of 34–35 °C is within the range of physiological variations on the upper arm under normal conditions (Freitas 1999). It was also shown by Barcroft and Edholm (Barcroft and Edholm 1943) that the effect of the local warming of the forearm on the skin blood flow can be observed for temperatures above 37 °C. Thus, we can conclude that the warming effect of the multisensor on the underlying skin is negligible.

Alternatively, significant increase of CBC during the first 2–3 h can be explained by the effect of local pressure-induced vasodilation (PIV)-physiological response of the body to the non-noxious external pressure applied to the skin (Abraham *et al* 2001, Koïtka *et al* 2004, Bochmann *et al* 2005). Initially, pressure from the attached sensor causes withdrawal of blood from the underlying skin volume (Abraham *et al* 2001). In order to supply cutaneous layers with oxygen and to prevent local ischemia, the local blood supply is increased with miscrovascular dilation. This effect is slow evolving and was reported to last tenths of minutes (Abraham *et al* 2001).

Therefore, the inter-patient differences in the extent of the BCI change can be attributed to the differences in the pressure applied by the MGMS to the skin due to the differences in the size of the arm, length of attachment band, force applied for the band fastening and band stiffness itself.

The decline after the first 2.5 h can be related to the so-called die away effect, similar to the effect observed during the local heating (Barcroft and Edholm 1943, Minson *et al* 2001), when presumably the vasodilator substance is washed out because of the induced high blood flow. Minson *et al* (2001) suggested that this substance can be l-arginine, a precursor of nitric oxide, which is involved in both heat- (Minson *et al* 2001, Charkoudian *et al* 2002) and pressure-induced (Fromy *et al* 2000) vasodilation mechanisms. Barcroft and Edholm have observed the maximum at around 50–70 min after the start of the heating procedure (Barcroft and Edholm 1943) and also stated the dependence of the time of maximum appearance from the temperature applied to the skin, which also affects the amplitude of the maximal blood flow. In our case l-arginine reduction can be delayed, since the overall rate of vasodilation buildup is slower than in the case of local heating.

4. Conclusions and outlook

The optical sensor for non-invasive monitoring of skin blood content was designed in a scope of the MGMS development for compensation of CBC-related variations of skin dielectric properties with a goal to improve accuracy of glucose monitoring with the approach of dielectric spectroscopy.

The Monte Carlo simulation of the PDP has been employed for the optimization of sensor sensitivity to the CBC changes. It was observed in the simulation results that the path of detected photons of green wavelength in the upper vascular plexus increases with the increase of SDD before reaching maximum at around 3.5 mm and then starts to decay. The 75% level of the maximum pathlength in UVP is reached for $r > 1.5$ mm.

At the same time, infrared light starts to propagate through the muscle layer on its way to the detector starting at SDD of 2.2 mm and reaching 25% of the pathlength in UVP at 2.4 mm.

Thus, in order to maximize sensor sensitivity to CBC, while minimizing the sensitivity to the blood content changes in the muscle, the range 1.5–2.4 mm has to be chosen for the SDD.

The optical reflectance sensor based on these findings has been designed and tested in a laboratory environment and under real-life conditions in the outpatient study in patients with T1DM. Results indicate that the optical module is highly sensitive to CBC variations and is also able to reliably detect day-long trends of the body's physiological conditions as well as short-term effects produced by position changes and physical activities.

The initial statistically significant increase of the measured CBC under the sensor during 3 h after attachment has been observed for all 16 subjects. It might be related to the protective local vasodilation response to the mechanical pressure from the sensor (PIV). It is followed by the slower decline during the following hours, which can be attributed to the so-called die-away effect due to washing out of substance involved in vasodilator chain.

Future investigations will address the influence of the CBC, monitored with the optical sensors, on the dielectric properties of the skin and underlying tissue. These results will indicate whether distortions related to the variations in the skin hemodynamics can be suppressed in the glucose-related signals and help to improve the quality of a NIGM approach based on multiple sensors.

References

Abraham P, Fromy B, Merzeau S, Jardel A and Saumet J L 2001 Dynamics of local pressure-induced cutaneous vasodilation in the human hand *Microvasc. Res.* **61** 122–9

ADA 1999 American Diabetes Association: clinical practice recommendations 1999 *Diabetes Care* Suppl 1 **22** S1–114

Allen J 2007 Photoplethysmography and its application in clinical physiological measurement *Physiol. Meas.* **28** R1–39

Anderson R R, Hu J and Parrish J A 1981 *Bioengineering and the Skin* ed P A Payne and R Marks (Amsterdam: Kluwer Academic)

Arimoto H, Egawa M and Yamada Y 2005 Depth profile of diffuse reflectance near-infrared spectroscopy for measurement of water content in skin *Skin Res. Technol.* **11** 27–35

Barcroft H and Edholm O G 1943 The effect of temperature on blood flow and deep temperature in the human forearm *J. Physiol.* **102** 5–20

Bashkatov A N, Genina E A, Kochubey V I and Tuchin V V 2005 Optical properties of human skin, subcutaneous and mucous tissues in the wavelength range from 400 to 2000 nm *J. Phys. D: Appl. Phys.* **38** 2543–55

Bochmann R P, Seibel W, Haase E, Hietschold V, Rödel H and Deussen A 2005 External compression increases forearm perfusion *J. Appl. Physiol.* **99** 2337–44

Braverman I M 1995 *Bioengineering of the Skin: Cutaneous Blood Flow and Erythema* ed E Berardesca (Boca Raton, FL: CRC Press)

Caduff A, Livshits L, Hayashi Y and Feldman Y *et al* 2004 Cell membrane response on d-glucose studied by dielectric spectroscopy. Erythrocyte and ghost suspensions *J. Phys. Chem.* B **108** 13827–30

Caduff A, Talary M S, Mueller M, Dewarrat F, Klisic J, Donath M, Heinemann L and Stahel W 2009 Non-invasive glucose monitoring in patients with type 1 diabetes: a multisensor system combining sensors for dielectric and optical characterisation of skin *Biosens. Bioelectron.* **24** 2778–84

Charkoudian N, Vella A, Reed A S, Minson C T, Shah P, Rizza R A and Joyner M J 2002 Cutaneous vascular function during acute hyperglycemia in healthy young adults *J. Appl. Physiol.* **93** 1243–50

Cheong W F, Prahl S A and Welch A J 1990 A review of the optical properties of biological tissues *IEEE J. Quantum Electron.* **26** 2166–85

Cui W J, Ostrander L E and Lee B Y 1990 *In vivo* reflectance of blood and tissue as a function of light wavelength *IEEE Trans. Biomed. Eng.* **37** 632–9

Delpy D T, Cope M, Van Der Zee P, Arridge S, Wray S and Wyatt J 1988 Estimation of optical pathlength through tissue from direct time of flight measurement *Phys. Med. Biol.* **33** 1433–42

Despopoulos A and Silbernagl S 2003 *Color Atlas of Physiology* (Stuttgart: Thieme)

Diffey B L, Oliver R J and Farr P M 1984 A portable instrument for quantifying erythema induced by ultraviolet radiation *Br. J. Dermatol.* **111** 663–72

Douven L F A and Lucassen G W 2000 Retrieval of optical properties of skin from measurement and modeling the diffuse reflectance *Proc. SPIE; Laser-Tissue Interaction XI: Photochemical, Photothermal, and Photomechanical* **3914** 312–23

Feather J W, Ellis D J and Leslie G 1988 A portable reflectometer for the rapid quantification of cutaneous haemoglobin and melanin *Phys. Med. Biol.* **33** 711–22

Freitas R A J 1999 *Nanomedicine. Vol I: Basic Capabilities* (Austin, TX: Landes Bioscience)

Fromy B, Merzeau S, Abraham P and Saumet J L 2000 Mechanisms of the cutaneous vasodilator response to local external pressure application in rats: involvement of CGRP, neurokinins, prostaglandins and NO *Br. J. Pharmacol.* **131** 1161–71

Gambichler T, Matip R, Moussa G, Altmeyer P and Hoffmann K 2006 *In vivo* data of epidermal thickness evaluated by optical coherence tomography: effects of age, gender, skin type, and anatomic site *J. Dermatol. Sci.* **44** 145–52

Gordy E and Drabkin D L 1957 Spectrophotometric studies: XVI. Determination of the oxygen saturation of blood by a simplified technique, applicable to standard equipment *J. Biol. Chem.* **227** 285–99

Hamaoka T, McCully K K, Quaresima V, Yamamoto K and Chance B 2007 Near-infrared spectroscopy/imaging for monitoring muscle oxygenation and oxidative metabolism in healthy and diseased humans *J. Biomed. Opt.* **12** 062105

Hayashi Y, Livshits L, Caduff A and Feldman Y 2003 Dielectric spectroscopy study of specific glucose influence on human erythrocyte membranes *J. Phys. D: Appl. Phys.* **36** 369–74

Hertzman A B, Randall W C and Jochim K E 1947 Relations between cutaneous blood flow and blood content in the finger pad, forearm, and forehead *Am. J. Physiol.* **150** 122–32

Hiraoka M, Firbank M, Essenpreis M, Cope M, Arridge S R, Van Der Zee P and Delpy D T 1993a A Monte Carlo investigation of optical pathlength in inhomogeneous tissue and its application to near-infrared spectroscopy *Phys. Med. Biol.* **38** 1859–76

Hiraoka M, Firbank M, Essenpreis M, Cope M, Arridge S R, Van Der Zee P and Delpy D T 1993b A Monte Carlo investigation of optical pathlength in inhomogeneous tissue and its application to near-infrared spectroscopy *Phys. Med. Biol.* **38** 1859–76

Hunter J A A, Savin J A and Dahl M V 2002 *Clinical Dermatology* (Oxford: Blackwell)

Iino K, Maruo K, Arimoto H, Hyodo K, Nakatani T and Yamada Y 2003 Monte Carlo simulation of near infrared reflectance spectroscopy in the wavelength range from 1000 nm to 1900 nm *Opt. Rev.* **10** 600–6

Khalil O S 2004 Non-invasive glucose measurement technologies: an update from 1999 to the dawn of the new millennium *Diabetes Technol. Ther.* **6** 660–97

Koïtka A, Abraham P, Bouhanick B, Sigaudo-Roussel D, Demiot C and Saumet J L 2004 Impaired pressure-induced vasodilation at the foot in young adults with type 1 diabetes *Diabetes* **53** 721–5

Kumar G and Schmitt J M 1997 Optimal probe geometry for near-infrared spectroscopy of biological tissue *Appl. Opt.* **36** 2286–93

Lima A and Bakker J 2005 Noninvasive monitoring of peripheral perfusion *Intensive Care Med.* **31** 1316–26

Meglinski I V and Matcher S J 2002 Quantitative assessment of skin layers absorption and skin reflectance spectra simulation in the visible and near-infrared spectral regions *Physiol. Meas.* **23** 741–53

Meglinskii I and Matcher S 2001 Analysis of the spatial distribution of detector sensitivity in a multilayer randomly inhomogeneous medium with strong light scattering and absorption by the Monte Carlo method *Opt. Spectrosc.* **91** 654–9

Meglinsky I V and Matcher S J 2001 Modelling the sampling volume for skin blood oxygenation measurements *Med. Biol. Eng. Comput.* **39** 44–50

Minson C T, Berry L T and Joyner M J 2001 Nitric oxide and neurally mediated regulation of skin blood flow during local heating *J. Appl. Physiol.* **91** 1619–26

Nilsson G E, Salerud E G, Strömberg T and Wårdell K 2003 *Biomedical Photonics Handbook* ed T Vo-Dinh (Boca Raton, FL: CRC Press)

Pearse A D, Edwards C, Hill S and Marks R 1990 Portable erythema meter and its application to use in human skin *Int. J. Cosmet. Sci.* **12** 63–70

Prahl S 1999 Optical absorption of hemoglobin http://omlc.ogi.edu/spectra/hemoglobin/index.html (date last accessed 22 June 2009)

Rhoades A and Bell D R 2008 *Medical Physiology: Principles for Clinical Medicine* (Philadelphia, PA: Lippincott Williams & Wilkins)

Sandberg M, Zhang Q, Styf J, Gerdle B and Lindberg L-G 2005 Non-invasive monitoring of muscle blood perfusion by photoplethysmography: evaluation of a new application *Acta Physiol. Scand.* **183** 335–43

Scanlon V C and Sanders T 2006 *Essentials of Anatomy and Physiology* (Philadelphia, PA: F A Davis)

Sinichkin Y P, Kollias N, Zonios G, Utz S R and Tuchin V V 2002 *Handbook of Optical Biomedical Diagnostics* ed V V Tuchin (Bellingham: SPIE Press) pp 727–85

Svaasand L, Norvang L, Fiskerstrand E, Stopps E, Berns M and Nelson J 1995 Tissue parameters determining the visual appearance of normal skin and port-wine stains *Lasers Med. Sci.* **10** 55–65

Talary M S, Dewarrat F, Huber D and Caduff A 2007 *In vivo* life sign application of dielectric spectroscopy and non-invasive glucose monitoring *J. Non-Cryst. Solids* **353** 4515–7

Wang L, Jacques S L and Zheng L 1995 MCML–Monte Carlo modeling of light transport in multi-layered tissues *Comput. Methods Programs Biomed.* **47** 131–46

Yun-Han L, Fu-Rong H, Shi-Ping L and Zhe C 2008 Detection limit of glucose concentration with near-infrared absorption and scattering spectroscopy *Chinese Phys. Lett.* **25** 1117–9

Zakharov P and Scheffold F 2009 *Light Scattering Reviews 4* ed A A Kokhanovsky (Heidelberg: Springer)